Assembly of 1,3,5-tris(2-alkylthiol-pyrimidin-4-yl)benzene) (alkyl = Me, n-Pr) with copper(I) iodide: effect of alkyl side chain

Hai-Bin Zhu & Lei Liang

View supplementary material ⊡

Accepted author version posted online: 22 Jan 2015.
Published online: 17 Feb 2015.

Submit your article to this journal ⊡

Article views: 60

View related articles ⊡

View Crossmark data ⊡

Taylor & Francis
Taylor & Francis Group

Assembly of 1,3,5-tris(2-alkylthiol-pyrimidin-4-yl)benzene) (alkyl = Me, n-Pr) with copper(I) iodide: effect of alkyl side chain
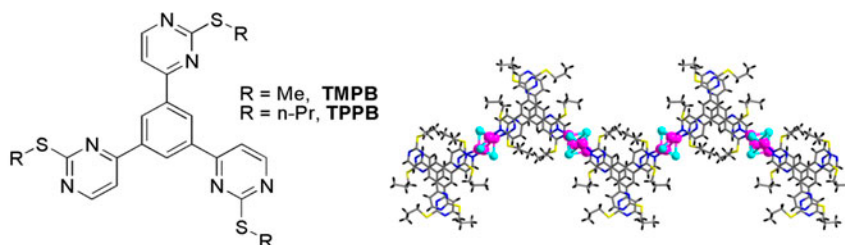
HAI-BIN ZHU* and LEI LIANG

School of Chemistry and Chemical Engineering, Southeast University, Nanjing, China

The side chain of organic building blocks can modulate the assembly of coordination polymer with respect to the assembly structure and packing alignment.

Two π-conjugated organic building blocks, **TMPB** and **TPPB** (**TMPB** = 1,3,5-tris(2-methylthiol-pyrimidin-4-yl)benzene; **TPPB** = 1,3,5-tris(2-propylthiol-pyrimidin-4-yl)benzene), have been prepared which only differ in the length of linear side chain attached to sulfur. Structural comparison between complexes of **TMPB** and **TPPB** reveals that the side chain has a great effect in modulating both the molecular structure and the molecular alignment. Reactions of **TMPB** and **TPPB** with CuI under the same conditions show that the side chain can exert impact on the assembly of coordination polymer. Assembly reaction with CuI is sensitive to the change in length of side chain, that is the shorter the side chain, the faster the reaction. Reaction of **TPPB** with CuI gives a 1-D chain structure of $[Cu_4I_4(\mathbf{TPPB})_2]_n$ (**1**) based on two distinctive Cu_4I_4 clusters, whilst only microcrystalline powder or precipitate can be obtained for **TMPB**. The side chain can, thus, tune the assembly of coordination polymer in terms of the assembly structure as well as its packing manner.

Keywords: Coordination polymer; Side chain effect; Crystal structure

1. Introduction

Crystal engineering of coordination polymers is of interest for diverse topologies with beauty and numerous potential applications [1, 2]. Great achievements have been made to tailor the structure and function of coordination polymers by means of the core functionalization of organic component, since the inner coordination information with organic building

---

*Corresponding author. Email: zhuhaibin@seu.edu.cn

block can be altered in this way, which would lead to significant structural variations of coordination polymers. By contrast, less attention has been paid to the periphery of organic building blocks such as the attached side chain [3, 4]. However, the side chain effect has been widely used as an elegant tool to finely modulate the molecular packing that is associated with the final solid-state properties of organic materials [5–8].

In our previous work, we designed an ethyl side-chain-decorated quasi-planar π-conjugated organic synthon **TEPB** (chart 1), which led to a 1-D flattened coordination chain based on Cu_4I_4 cluster upon reaction of CuI [9]. To investigate the side chain effect on the assembly of coordination polymers, herein we prepared two analogs of **TEPB** – **TMPB** and **TPPB** – which only differ in the length of the linear side chain (**TMPB**: methyl side chain; **TPPB**: n-propyl side chain) (chart 1). The length of the side chain might influence the coordination ability of the pyrimidinyl ring due to change in steric hindrance, which would further affect the assembly of the coordination polymer. The side chain variation is also expected to modulate the packing structure of coordination polymers as seen in organic materials.

2. Experimental

2.1. *Materials and measurements*

All solvents and reagents of analytical grade were used as received. The starting material P3 (1,3,5-tris(2-thio-pyrimidin-4-yl)benzene) for preparation of **TMPB** and **TPPB** was obtained according to our reported procedure [9]. IR spectra were recorded with a Thermo Scientific Nicolet 5700 FT-IR spectrophotometer with KBr pellets from 400 to 4000 cm^{-1}. ^{1}H NMR spectra were recorded with a Bruker AVANCE-500 spectrometer. Electrospray ionization (ESI) mass spectra were recorded with a Finnigan MAT SSQ 710 mass spectrometer from 100 to 1200 amu. Elemental analyses for C, H, and N were performed on a CHN–O-Rapid analyzer and an Elementar Vario MICRO analyzer. Powder X-ray diffraction (PXRD) data were recorded on a Siemens Bruker D5000 X-ray powder diffractometer equipped with Cu-$K\alpha$ radiation, with a step size and a scan speed of 0.02° and 5° min^{-1}, respectively. Simulated PXRD pattern was calculated with the Mercury program using the single crystal data. Solid-state UV–vis absorption spectra were recorded with a Shimadzu UV-2450 UV–vis spectrophotometer. The direct current (dc) conductivity of **1** were measured on pressed powder pellet samples (the thickness of $d = 0.80$ mm) sandwiched by a square brass electrode (10×10 mm^2) with a CHI660D (Chenghua, Shanghai) electrochemistry workstation, wherein the applied dc voltages varied from 0 to 10 V.
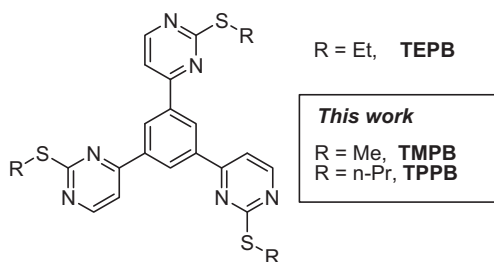

Chart 1.   Organic ligands of **TMPB** and **TPPB**.

2.2. *Synthesis*

2.2.1. Synthesis of TMPB and TPPB. At room temperature, sodium metal (2.1 g, 90.0 mM) was slowly added into 50 mL of anhydrous EtOH to give a clear colorless solution. P3 (2.0 g, 5.0 mM) was then added into the solution and stirred for 40 min to form a cloudy solution. On addition of MeI (28.0 g, 180.0 mM), the resulted solution was stirred overnight at the same temperature. The reaction was quenched by addition of 150 mL of water. The resultant precipitate was filtered and washed thoroughly with water. Upon decolorization with active carbon in $CHCl_3$ solvent, the final product of **TMPB** was afforded as pale yellow solid. Single crystals of **TMPB** suitable for X-ray diffraction were obtained by slow evaporation of its acetone solution. **TPPB** was afforded in an analogous manner, only replacing MeI with n-PrI. Quality single crystal of **TPPB** was obtained by slow diffusion of MeOH into its CH_2Cl_2 solution.

TMPB: Yield 35%. IR (KBr, cm^{-1}): 2927w, 1552s, 1444s, 1415m, 1388s, 1340m, 1311m, 1272w, 1207m, 1183m, 1126w, 971w, 904w, 820m, 790w, 772w, 741w, 719w, 677w, 636m, 628m. ^{1}H NMR (CDCl$_3$/TMS, 500 MHz, ppm): δ 8.93 (s, 3H), 8.65 (d, 3H), 7.52 (d, 3H), 2.60 (s, 9H). MS (ESI): m/z (%) = 451 (100) [M + H]$^+$. Anal. $C_{21}H_{18}N_6S_3$ (%): Calcd C, 55.97; H, 4.03; N, 18.65. Found: C, 55.81; H, 3.95; N, 18.54.

TPPB: Yield 32%. IR (KBr, cm^{-1}): 2964m, 2925m, 2871w, 1554vs, 1453s, 1394s, 1358w, 1328s, 1270w, 1202s, 1182m, 1119w, 1065w, 899m, 822s, 774w, 737m, 717m, 682w, 632m, 482w. ^{1}H NMR (CDCl$_3$/TMS, 500 MHz, ppm): δ 8.87 (s, 3H), 8.62 (d, 3H), 7.49 (d, 3H), 3.24 (t, 6H), 1.86 (m, 6H), 1.11 (m, 9H). ESI-MS: m/z (%) = 535 (100) [M + H]$^+$. Anal. $C_{27}H_{30}N_6S_3$ (%): Calcd C, 60.64; H, 5.65; N, 15.72. Found: C, 60.92; H, 5.58; N, 15.66.

2.2.2. Preparation of 1, $[Cu_4I_4(TPPB)]_n$. A CH_3CN solution (3.0 mL) containing CuI (0.06 mM) was carefully layered above a CH_2Cl_2 solution (3.0 mL) of **TPPB** (0.02 mM), wherein 5.0 mL of H_2O as a buffer layer was placed between them. A quantity of crystals was afforded in a period of one month. A single crystal suitable for X-ray diffraction analysis was selected from the bulk crystals.

Yield 40% (based on **TPPB**). IR (KBr, cm^{-1}): 2957w, 2925w, 2868w, 1642w, 1561vs, 1446w, 1415m, 1386s, 1347s, 1325m, 1270w, 1202m, 1176m, 1119w, 1087w, 899w, 820m, 770w, 732w, 681w, 632w. Anal. $C_{54}H_{60}Cu_4I_4N_{12}S_6$: Calcd C, 35.42; H, 3.30; N, 9.18%. Found: C, 35.55; H, 3.60; N, 9.38%.

2.3. *X-ray crystallography*

Diffraction intensity data for **TMPB**, **TPPB**, and **1** were collected at 298(2) K on a Bruker SMART CCD-4K diffractometer employing graphite-monochromated Mo-Kα radiation ($\lambda = 0.71073$ Å). The data were collected using SMART and reduced by the program SAINT [10]. All the structures were solved by direct methods and refined by full-matrix least squares on F_{obs}^2 by using the SHELXTL-PC software package [11]. All non-hydrogen atoms were refined anisotropically. All hydrogens were calculated by geometrical methods and refined as a riding model. The crystallographic data for **TMPB**, **TPPB**, and **1** are listed in table 1.

Table 1. Crystallographic data for **TMPB**, **TPPB,** and **1**.

Compound	**TMPB**	**TPPB**	**1**
Formula	$C_{21}H_{18}N_6S_3$	$C_{27}H_{30}N_6S_3$	$C_{54}H_{60}Cu_4I_4N_{12}S_6$
Mr	450.59	534.78	1831.36
Crystal system	Monoclinic	Triclinic	Monoclinic
Space group	$P2_1/n$ (No. 14)	P-1 (No. 2)	$P2_1/c$ (No. 14)
a (Å)	12.055(1)	7.620(1)	25.655(3)
b (Å)	8.510(1)	12.497(2)	15.589(2)
c (Å)	20.584(2)	15.040(2)	16.512(2)
α (°)	90	93.072(2)	90
β	91.494(2)	97.369(2)	91.472(1)
γ	90	99.837(2)	90
V (Å^3)	2110.8(4)	1395.3(4)	6601(1)
Z	4	2	4
D_{Calcd} (g cm^{-3})	1.418	1.273	1.843
$F(0\,0\,0)$	936	564	3568
Reflns. collected	14,419	9940	47,022
Unique reflns.	3719	4851	12,227
R (int)	0.038	0.017	0.076
R_1, wR_2 [$I > 2\sigma(I)$]	0.0414/0.1032	0.0473/0.1159	0.0581/0.1466
R_1, wR_2 (all data)	0.0664/0.1127	0.0666/0.1252	0.1066/0.1748
GOF	1.05	1.02	1.06

3. Results and discussion

3.1. *Synthesis and characterization of TMPB and TPPB*

The preparation of **TMPB** and **TPPB** is almost identical to that for **TEPB** [9], which only differs in the alkylating agent (**TMPB**: CH$_3$I; **TPPB**: n-PrI). **TMPB** and **TPPB** have been characterized by ^{1}H NMR, ESI-MS, and elemental analysis, which are in accord with their formulas. ^{1}H NMR spectrum of **TMPB** in CDCl$_3$ shows a singlet of the central phenyl proton at $\delta = 8.93$ ppm and two resonances at $\delta = 8.65$ and 7.52 ppm corresponding to
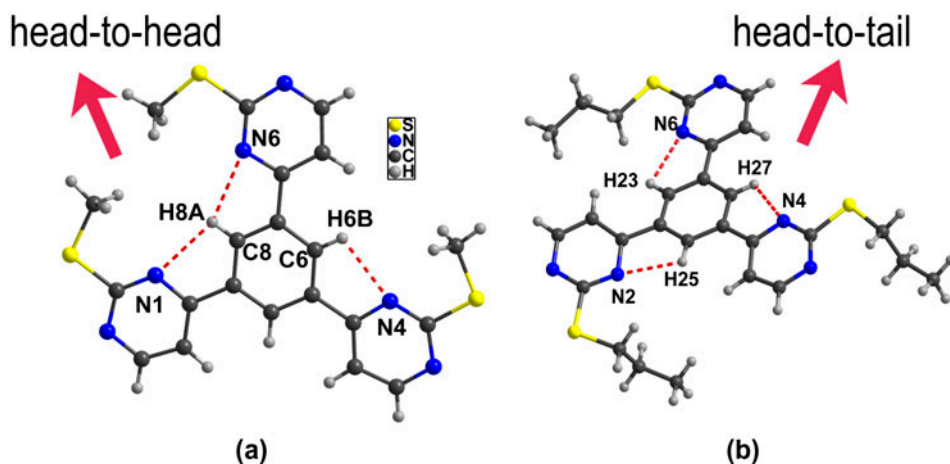

Figure 1. Crystal structure of **TMPB** (a) and **TPPB** (b) (Intramolecular hydrogen bonds denoted by red dashed lines. C6–H6B···N4: C6···N4 2.736(3) Å, C6–H6B···N4 102°; C8–H8A···N1: C8···N1 2.775(3) Å, C8–H8A···N1 101°; C8–H8A···N6: C8···N6 2.806(3) Å, C8–H8A···N6 101°. C5–H5A···N2: 2.896(3) Å, C5···N2 102°; C23–H23···N6: 2.766(3) Å, C23···N6 102°; C27–H27···N4: C27···N4 2.768(3) Å, C27–H27···N4 101°) (see http://dx.doi.org/10.1080/00958972.2015.1011147 for color version).

pyrimidine protons. The methyl protons of **TMPB** are at $\delta = 2.60$ ppm. Compared to **TMPB**, the ^{1}H NMR resonances of the central phenyl and pyrimidine protons for **TPPB** are at $\delta = 8.87$, 8.62, and 7.49 ppm, respectively. The n-propyl groups show three separated signals at $\delta = 3.24$, 1.86, and 1.11 ppm. The ESI-MS spectra of **TMPB** and **TPPB** exhibit signals at $m/z = 451$ and 535, which match well with the protonated **TMPB** and **TPPB**, respectively.

The crystal structures of **TMPB** and **TPPB** have been elucidated by single-crystal X-ray diffraction. **TMPB** crystallizes in monoclinic space group $P21/n$. As depicted in figure 1(a), there exist intramolecular C–H···N hydrogen bonds in **TMPB**, which restrict the rotation of pyrimidinyl rings with respect to the central phenyl ring, forming relatively small dihedral angles (5.26°, 5.33°, and 9.17°) between them. As a consequence, **TMPB** can be viewed as a quasi-planar organic building block. Different from **TEPB**, one pyrimidinyl ring in **TMPB** was flipped from one face to the other face, enabling two pyrimidinyl rings to orient in a head-to-head fashion. **TPPB** crystallizes in triclinic space group P-1. As depicted in figure 1(b), **TPPB** also features intramolecular C–H···N hydrogen bonds, which limit the range of the corresponding dihedral angles from 2.95° to 18.67°. Analogous to **TEPB**, three pyrimidinyl rings in **TPPB** are uniformly arrayed in a head-to-tail manner. The different orientation of pyrimidinyl rings between **TMPB** and **TPPB** is relevant to the difference in steric bulk between methyl and propyl side chains.

Although **TMPB** and **TPPB** are similar in their molecular structures, they exhibit quite different molecular packing. A typical herringbone arrangement was observed with **TMPB**, wherein intermolecular C–H···S contacts [12, 13] and aromatic π–π* interactions exist (figure 2). By constrast, a face-to-face molecluar stacking was found with **TPPB** which involves C–H···N interactions together with aromatic stacking interactions (figure 3). By

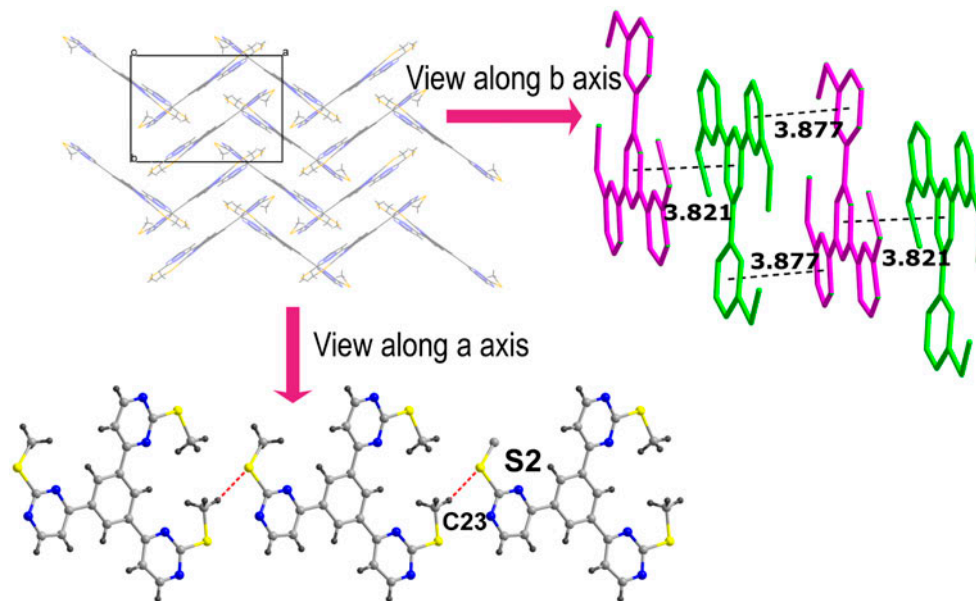Figure 2. Molecular packing of **TMPB** (C–H···S interactions denoted by red dashed lines. C23–H23A···S2: C23···S2, 3.632(3) Å; C23–H23A···S2 163°; asymmtric code $1 + x$, $-1 + y$, z) (see http://dx.doi.org/10.1080/00958972.2015.1011147 for color version).
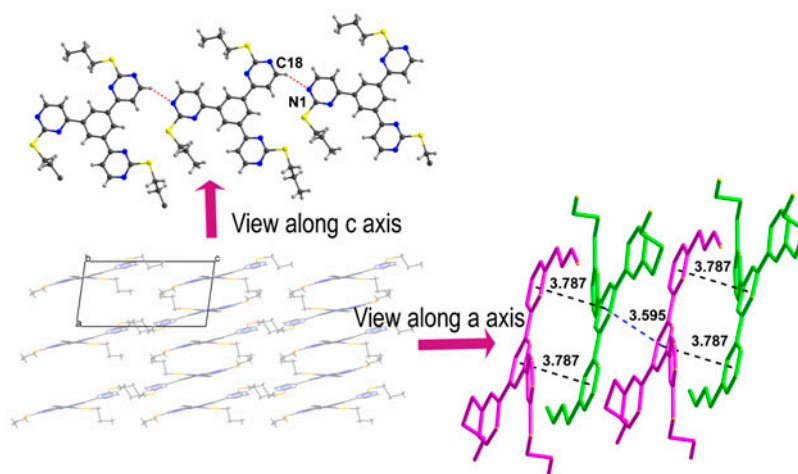
Figure 3. Molecular packing of **TPPB** (C–H⋯N interactions denoted by red dotted lines. C18–H18⋯N1: C18⋯N1 3.313(3); C18–H18⋯N1 148°; asymmetric code *x*, 1 + *y*, *z*) (see http://dx.doi.org/10.1080/00958972.2015.1011147 for color version).

comparison of **TMPB** and **TPPB** with the reported **TEPB** [9], a small change in the side chain length is seen to have an impact on molecular structures especially solid-state packing. First, the side chain variation influences their molecular conformation despite sharing some common points (e.g. intramolecular C–H⋯N hydrogen bonds). According to the average dihedral angle between the outer pyrimidinyl ring and the central phenyl ring, the molecule exhibits a larger deviation from the quasi-planar conformation with increasing length in the side chain, which is caused by increasing steric crowding with longer side chains. Second, the molecular packing can be evidently changed by the side chain length. When the side chain was lengthened from methyl through ethyl to propyl, the molecule aggregation varies from herringbone arrangement (for **TMPB**) through 2-D C–H⋯S hydrogen-boned layer (for **TEPB**) to face-to-face arrangement (for **TPPB**).

3.2. *Preparation and structural description of 1*

For better understanding of the side chain effect on the assembly of a coordination polymer, assembly of CuI with **TMPB** and **TPPB** was carried out under the same conditions as described for **TEPB** [9]. The assembly reaction is susceptible to the length of the side chain, that is, the shorter the side chain, the faster the reaction. It was a challenge to grow suitable single crystals for **TMPB**, which gives either solid precipitate or microcrystalline powder though many attempts were made (Supporting information). For **TPPB**, the assembly reaction proceeds smoothly, from which quality single crystals of **1** formed at the bottom of the reaction vessel over one month. It is not surprising that the slower reaction for **TPPB** than **TMPB** is caused by lowered coordination activity of pyrimidinyl rings due to the steric blockage by the larger propyl group. Moreover, the better solublizing ability with propyl side chain than the methyl counterpart may also benefit crystal formation, preventing rapid formation of precipitate. The phase purity of the as-synthesized samples of **1** was confirmed by the consistency between the experimental PXRD pattern and the simulated PXRD pattern (figure 4).
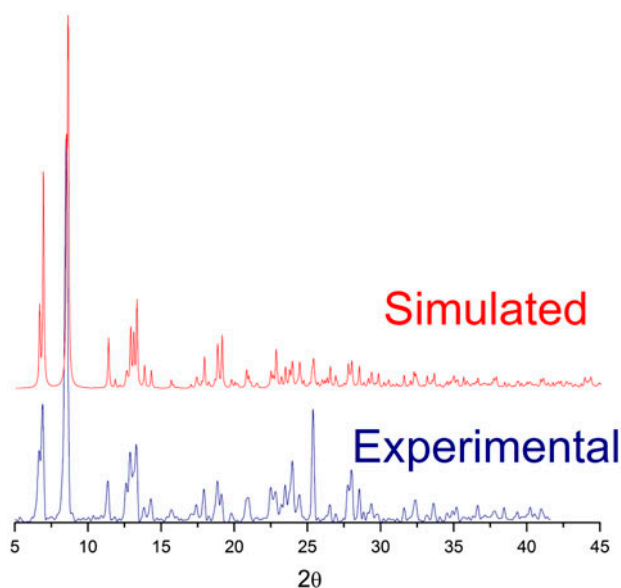
Figure 4. Comparison between the experimental PXRD pattern and the simulated PXRD pattern of **1**.
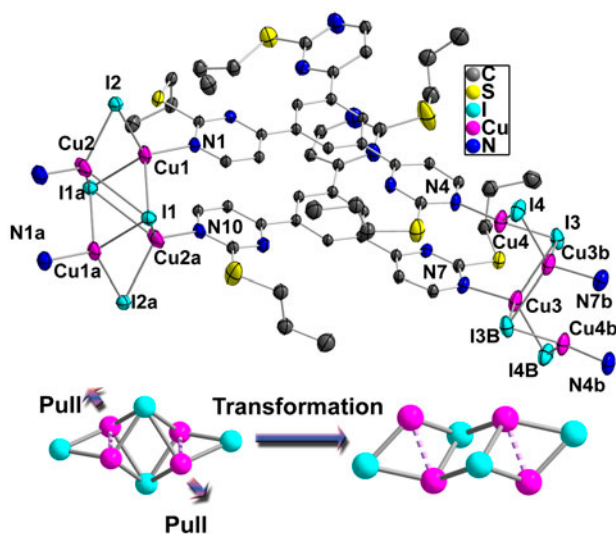

Figure 5. Coordination environment of two distinctive Cu_4I_4 clusters ($Cu\cdots Cu$ interactions denoted by dotted line).

Single-crystal X-ray crystallography shows that **1** crystallizes in monoclinic space group $P2(1)/c$. The asymmetric unit of **1** is composed of four tetrahedral Cu ions, four iodides, and two **TPPB** ligands. As shown in figure 5, there exist two disparate forms of Cu_4I_4 clusters in **1**. One involves two $\mu^2\text{-}I^-$ and two $\mu^4\text{-}I^-$, wherein four Cu ions form an approximate

rectangle with Cu–Cu sides being 2.448 and 3.153 Å. Two μ^4-I$^-$ are displaced by 2.0082(6) Å above and below the Cu$_4$-defined plane with Cu–I distances varying from 2.679 to 3.056 Å. Two μ^2-I$^-$ are situated near the short sides of the Cu$_4$-rectangle with two Cu–I bond lengths of 2.591 and 2.611 Å. The shape of the Cu$_4$I$_4$ cluster appears as a basket, which resembles that in $\{[(\mathbf{TEPB})Cu_2I_2] \cdot CH_3CN\}_n$ [9]. The other with a step-like shape can be regarded as a mutant of the former one, which can be transformed by pulling the former Cu$_4$I$_4$ cluster along one diagonal line of the Cu$_4$-rectangle. The operation makes the original Cu$_4$-rectangle a parallelogram with two Cu–Cu sides being 2.521 and 3.542 Å. It is composed of two μ^3-I$^-$, two μ^2-I$^-$, two tetrahedral Cu ions, and two trigonal Cu ions. Two μ^3-I$^-$ ions are located at 1.9265(6) Å above and below the Cu$_4$-defined plane with Cu–I distances varying from 2.629 to 2.758 Å. Two μ^2-I$^-$ are near the short sides of the Cu$_4$-parallelogram with two Cu–I bonds of 2.501 and 2.611 Å. For the two types of Cu$_4$I$_4$ clusters, the remarkably short Cu···Cu separations (Cu1···Cu2: 2.448(2) Å; Cu3···Cu4 2.521(2) Å) indicate the presence of weak Cu···Cu interaction. In crystal engineering, copper(I) halide has been extensively employed as a versatile inorganic node, because its aggregates can adopt different geometries [14]. Coexistence of two geometrically distinctive Cu$_4$I$_4$ clusters in one coordination polymer is rare. Although two Cu$_4$I$_4$ clusters both serve as the four-connecting node linking four **TPPB** ligands *via* Cu–N coordination bonds (Cu1–N1: 1.993(6) Å; Cu2–N10a: 1.996(6) Å); Cu3–N7: 2.032(6) Å; Cu4–N4: 1.973(6) Å), the almost linear N–Cu–Cu–N connectivity limits the dimension of the coordination polymer. Consequently, the two Cu$_4$I$_4$ clusters are spaced by a pair of **TPPB** ligands, which are stacked in an eclipsed manner. Each **TPPB** is a normal organic bridge with one pyrimidinyl ring free of coordination. Irrespective of the presence of intramolecular C–H···N hydrogen bonds in these coordinated **TPPB** ligands, a marked rotation of the free pyrimidinyl ring against the central phenyl ring is observed with the formation of a large dihedral angle (27.40° and 32.95°). The repeated connection between Cu$_4$I$_4$ inorganic nodes and **TPPB** pairs along one direction resulted in a 1-D chain structure, in which two different Cu$_4$I$_4$ clusters are alternatively arrayed in a linear fashion (figure 6).

The variation in side chain length not only influences the assembly of the coordination polymer but also packing manner. Although all 1-D coordination chains of **1** are parallel to each other along one plane, the interchain S···S or C–H···S interactions are not present
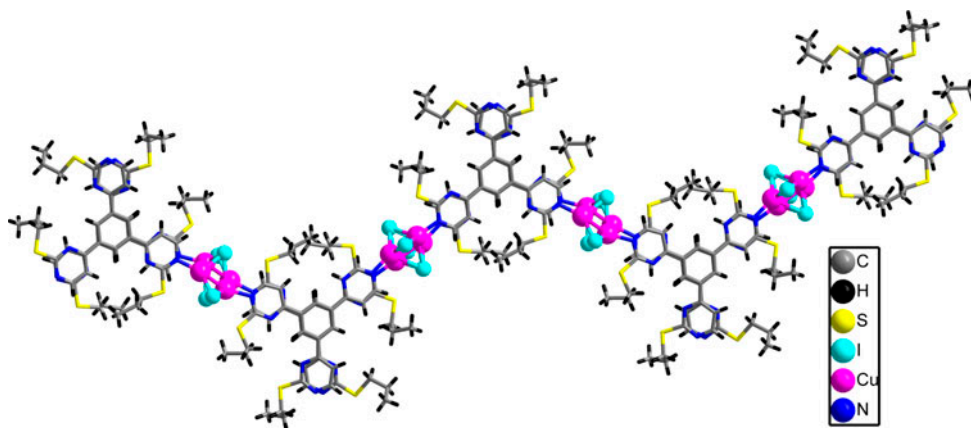

Figure 6. 1-D chain structure of **1**.

which have been observed in our previously reported $\{[(\textbf{TEPB})Cu_2I_2]\cdot CH_3CN\}_n$ and $\{[(\textbf{TEPB})CuCl_2]\cdot H_2O\}_n$ [9]. Such a difference in the packing of **1** is ascribed to the increasing interchain steric repulsion as the increase in side chain length, wherein the shortest interchain S···S and C···S separations are extended to 4.142 and 3.831 Å, respectively.

3.3. *UV–vis spectroscopic and conductive properties of 1*

The UV–vis absorption of **1** was examined in solid state at room temperature. As shown in figure 7, the absorption spectra of **1** show two major absorptions with a shoulder at 224, 365, and 447 nm, respectively. The absorptions at 224 and 365 nm are assigned to ligand-centered transitions (π–π* and n–π* transition), whereas the shoulder at 447 nm might originate from the metal-to-ligand charge-transfer. Compared to the UV–vis absorptions of $\{[(\textbf{TEPB})Cu_2I_2]\cdot CH_3CN\}_n$ (230, 382, and 466 nm), a blue-shift is clearly seen in **1**, which infers a larger HOMO-LUMO gap. Following the equation $Eg = 1240/\lambda$ (absorption edge) [15], the HOMO-LUMO gap (Eg = band gaps) of **1** was estimated at 2.06 eV from its absorption edge (602 nm), which is a little larger than that (1.93 eV) of $\{[(\textbf{TEPB})Cu_2I_2]\cdot CH_3CN\}_n$. The rising Eg with **1** may be in part ascribed to significant deviation of **TPPB** ligands from quasi-planar conformation, which disrupts the π-conjugation. Copper(I) iodide has been used to construct coordination polymers with conductive properties owing to its intrinsic semiconductive nature [16–19]. However, it was found that $\{[(\textbf{TEPB})Cu_2I_2]\cdot CH_3CN\}_n$ behaves as an insulator. Given the larger HOMO-LUMO gap of **1** than $\{[(\textbf{TEPB})Cu_2I_2]\cdot CH_3CN\}_n$, the conductivity of **1** is expected to be fairly poor. Figure 7 (inset) depicts the current–voltage (I–V) curve of **1**, and the dc electrical conductivity (σ_{dc}) was calculated according to the equation: $\sigma_{dc} = I/V \times d/S$ (where d is the thickness of the pellet sample and S is the electrode area); **1** is resistant to electrical conduction with a room-temperature dc conductivity of 10.41×10^{-12} S cm^{-1}.
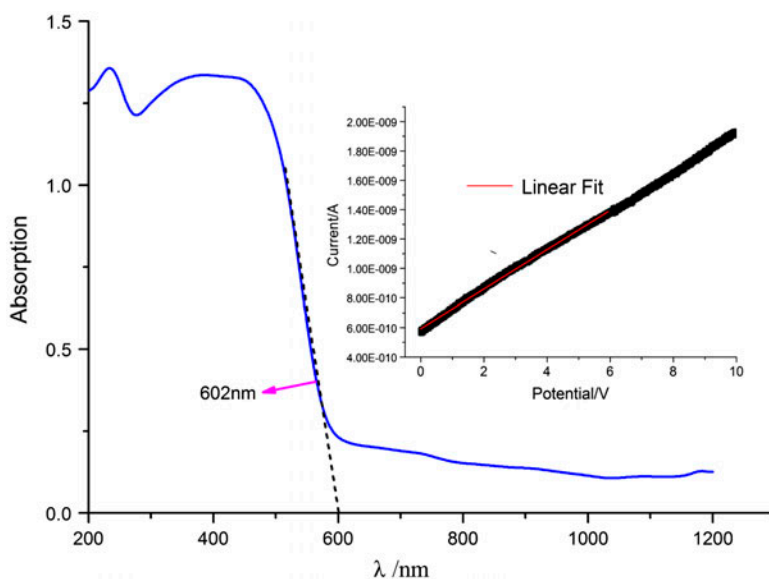

Figure 7.   The UV–vis absorption properties of **1** (inset: I–V curve of **1**).

4. Conclusion

Two organic building blocks with different length of side chains, **TMPB** and **TPPB**, have been prepared for studying side chain effects. Structural comparison between **TMPB** and **TPPB** reveals that the side chain can modulate both their molecular structure and their alignment. Assembly reaction with CuI further demonstrates the side chain effect on the assembly of the coordination polymer. The side chain can influence the rate of assembly reaction due to different steric bulk effects and can also tune the assembly of coordination polymer in terms of the assembly structure and packing. The study shows that the side chain effect can be employed as a valuable tool for crystal engineering of coordination polymers.

Supplementary material

CCDC-1017963 (for **1**), -1017964 (for **TMPB**) and -1017965 (for **TPPB**) contain the supplementary crystallographic data for this article. These data can be obtained free of charge via http://www.ccdc.cam.ac.uk/conts/retrieving.html, or from the Cambridge Crystallographic Data Center, CCDC, 12 Union Road, Cambridge CB2 1EZ, UK (Fax: 44-1223-336-033; or E-mail: deposit@ccdc.cam.ac.uk).

Funding

Supplemental data

Supplemental data for this article can be accessed here [http://dx.doi.org/10.1080/00958972.2015.1011147].

References

[1] M.C. Hong, L. Chen. *Design and Construction of Coordination Polymers*, John Wiley & Sons, Hoboken, NJ (2009).
[2] B. Moulton, M.J. Zaworotko. *Chem. Rev.*, **101**, 1629 (2001).
[3] J. He, M. Zeller, A.D. Hunter, Z. Xu. *J. Am. Chem. Soc.*, **134**, 1553 (2012).
[4] L. Li, J.M. Yue, Y.Z. Qiao, Y.Y. Niu, H.W. Hou. *CrystEngComm*, **15**, 3835 (2013).
[5] F. May, V. Marcon, M.R. Hansen, F. Grozema, D. Andrienko. *J. Mater. Chem.*, **21**, 9538 (2011).
[6] K. Balakrishnan, A. Datar, T. Naddo, J. Huang, R. Oitker, M. Yen, J. Zhao, L. Zang. *J. Am. Chem. Soc.*, **128**, 7390 (2006).
[7] A. Gadisa, W.D. Oosterbaan, K. Vandewal, J.C. Bolsée, S. Bertho, J. D'Haen, L. Lutsen, D. Vanderzande, J.V. Manca. *Adv. Funct. Mater.*, **19**, 3300 (2009).
[8] G. Chen, H. Sasabe, Y. Sasaki, H. Katagiri, X.F. Wang, T. Sano, Z. Hong, Y. Yang, J. Kido. *Chem. Mater.*, **26**, 1356 (2014).
[9] H.B. Zhu, R.Y. Shan, Y.F. Wu, Y.B. Lou. *Eur. J. Inorg. Chem.*, 1356 (2014).
[10] Siemens. *SAINT (Version 4) Software Reference Manual*, Siemens Analytical X-ray Systems, Inc., Madison, WI (1996).
[11] Siemens. *SHELXTL (Version 5), Reference Manual*, Siemens Analytical X-ray Systems, Inc., Madison, WI (1996).

[12] M. Domagała, S.J. Grabowski. *J. Phys. Chem. A*, **109**, 5683 (2005).
[13] M.J. Potrzebowski, M. Michalska, A.E. Kozioł, S. Każmierski, T. Lis, J. Pluskowski, W. Ciesielski. *J. Org. Chem.*, **63**, 4209 (1998).
[14] R. Peng, M. Li, D. Li. *Coord. Chem. Rev.*, **1**, 254 (2010).
[15] A.B. Murphy. *Sol. Energy Mater. Sol. Cells*, **91**, 1326 (2007).
[16] Y. Chen, Z.Q. Wang, Z.G. Ren, H.X. Li, D.X. Li, D. Liu, Y. Zhang, J.P. Lang. *Cryst. Growth Des.*, **9**, 4963 (2009).
[17] H.B. Zhu, Y.D. Chen, W.N. Yang. *J. Inorg. Organomet. Polym.*, **23**, 793 (2013).
[18] H.B. Zhu, W.N. Yang, R.Y. Shan. *J. Coord. Chem.*, **66**, 435 (2013).
[19] S.L. Li, X.M. Zhang. *Inorg. Chem.*, doi: 10.1021/ic500822w.